Delft University of Technology

Document Version
Final published version

Citation (APA)
Du, L., Zhao, X., Poelma, R. H., van Driel, W. D., & Zhang, G. Q. (2024). Health Monitoring Fatigue Properties of Solder Interconnects in LED Drivers. In *Recent Advances in Microelectronics Reliability: Contributions from the European ECSEL JU Project iRel40* (pp. 339-354). Springer. https://doi.org/10.1007/978-3-031-59361-1_13

Important note
To cite this publication, please use the final published version (if applicable).
Please check the document version above.

Copyright
In case the licence states “Dutch Copyright Act (Article 25fa)”, this publication was made available Green Open Access via the TU Delft Institutional Repository pursuant to Dutch Copyright Act (Article 25fa, the Taverne amendment). This provision does not affect copyright ownership.
Unless copyright is transferred by contract or statute, it remains with the copyright holder.

Sharing and reuse
Other than for strictly personal use, it is not permitted to download, forward or distribute the text or part of it, without the consent of the author(s) and/or copyright holder(s), unless the work is under an open content license such as Creative Commons.

Takedown policy
Please contact us and provide details if you believe this document breaches copyrights.
We will remove access to the work immediately and investigate your claim.

This work is downloaded from Delft University of Technology.

Green Open Access added to TU Delft Institutional Repository

'You share, we take care!' - Taverne project

https://www.openaccess.nl/en/you-share-we-take-care

Otherwise as indicated in the copyright section: the publisher is the copyright holder of this work and the author uses the Dutch legislation to make this work public.

Chapter 13
Health Monitoring Fatigue Properties of Solder Interconnects in LED Drivers

L. Du, X. Zhao, R. H. Poelma, W. D. van Driel, and G. Q. Zhang

13.1 Introduction

Electronic components are connected to printed circuit boards (PCB) using solder connections. On the one hand, with the miniaturization of electronic products and the development of multi-functionality, solder spot size continues to decrease, meanwhile the chip size is growing to contain a higher number of solder joints. The use of electronic equipment has found an increasing number of applications such as military, aviation, aerospace, and other harsh environments. As such, solder joints are inevitably subjected to high temperature, high humidity, and vibration shock loads. These factors make the solder joint reliability an important issue and a significantly investigated topic of academic research [1]. Solder joint reliability is fundamentally attributed to the mismatch of material properties, e.g. the coefficient of thermal expansion (CTE), between the electronic components and the PCB [2, 3, 4].

In the past few years, the lead-free solder alloy (e.g. SnAg, SnAgCu) is widely used in electronic packaging, which has been a mainstream replacement of leaded

---

L. Du (✉) · G. Q. Zhang
Department of Microelectronics, Delft University of Technology, Delft, The Netherlands
e-mail: L.Du@tudelft.nl

X. Zhao
Signify Research, Eindhoven, The Netherlands

R. H. Poelma
Nexperia, Nijmegen, The Netherlands

W. D. van Driel
Department of Microelectronics, Delft University of Technology, Delft, The Netherlands

Nexperia, Nijmegen, The Netherlands
e-mail: willem.van.driel@signify.com

© The Author(s), under exclusive license to Springer Nature Switzerland AG 2024

W. D. van Driel et al. (eds.), *Recent Advances in Microelectronics Reliability*,
https://doi.org/10.1007/978-3-031-59361-1_13

solder alloys (PbSn) for environmental protection. To meet the increased demand for a longer lifetime of electronic components during their applications, the creep properties of the solder joint under high temperatures is one critical issue to address. Previous studies proposed to enhance the creep behaviours by adding fillers into base solder alloys [5–8]. For example, the addition of Cu to SnAg was reported to moderately enhance the creep resistance at both room temperature and elevated temperature [5]. The SnAg with Ni fillers presents a higher creep resistance at room temperature compared with SnAgCu alloys but has an insignificant effect under high temperature. Moreover, Shen et al. [6] studied the effect of nano-metallic fillers (Cu, Ni) on the creep properties of SnBi solder alloys. In that study, an optimum filler concentration for creep resistance enhancement is identified at which there is a balance between the effects of particle pinning and microstructure refinement [6].

Lead-free solder alloys (e.g. SnCu, SnAgCu) became mainstream as the interconnect solution and substituted the leaded solder alloys (SnPb) for environment protection. Many studies investigated the fatigue behaviour of SnAgCu solder alloys by combining experiments (e.g. thermal cycling and/or tensile fatigue tests) with finite element (FE) simulations. As input to those simulations, fatigue models are developed with good reviews given by Lee et al. [7], Wong et al. [8], and Schubert et al. [9]. Combining those fatigue models with detailed FE models would then reveal the cycles to failure for a specific package, be it ball grid array (BGA) or quad flat no-lead (QFN) packages. For example, Athamneh et al. [10] revealed that increasing the aging temperature and time would lead to lower fatigue resistance of SnAgCu solder alloys, which caused more damage per cycle and less number cycles to failure for solder interconnects. Alam et al. [11] performed high-temperature creep tests of SnAgCu solder alloys from 125 °C to 200 °C and found that there was a significant increase of secondary creep strain rate at higher temperatures. Sn-3.0Ag-0.5Cu (SAC305) is the most widely used solder alloys for electronic packaging with acceptable fatigue resistance and mechanical properties. It is known that the effect of creep on fatigue evolution can markedly decrease the lifetime. Samavatian et al. [12] revealed that the consideration of creep on fatigue process caused 34% difference in the lifetime prediction while comparison of the results for different solders shows that the addition of dopants (e.g. Bi, Ni, and Sb) in the traditional SAC alloys improves their properties significantly. Long et al. [13] revealed the current effects on the creep behaviour of this SAC305 solder. Recently, an alternative solder alloy (SnBiAgCu) with lower silver content is expected to substitute SAC305 solder alloys. It was reported by Dokoupil and Stary [14] that this solder alloy achieved higher shear strength than SAC305 solder alloy after the thermal stress tests. However, the detailed mechanical analysis of this solder alloy for various creep strain test conditions is still missing. Thus, it is important to evaluate different solder alloys in terms of tensile and creep properties experimentally so accurate numerical simulation methods can be performed with the correct material data.

Potting materials are used to protect the electronic components from harsh conditions, such as extreme temperatures, mechanical vibration, and humidity [15]. It was reported that there was a large reduction in fatigue life when shrink or expansion stresses exist in the solder due to the thermal expansion of the potting compounds [16]. It means that the potting compounds will accelerate the fatigue failure process of solder interconnects to some extent. Zhu et al. [17] studied the effect of viscoelasticity behaviour of potting compounds by changing the curing temperature. They concluded that potting compounds cured at lower temperature are prone to induce more stress-related damage than those cured at higher temperature. As such, our investigations will also include the effects of potting materials.

Prognostics and health monitoring (PHM) are not just about creating a more reliable product: it is about creating a more predictable product based on real-world usage conditions [18, 19, 20]. Data analytics is a necessary part of this but is not enough [21]. To add value, product insights need to be leveraged into the technologies that are used to differentiate from others. PHM is not about troubleshooting reliability issues; rather, it is a new control point enabled by the transition to a services business. It is the combination of data and deep physical (and technological) insight that will give a unique "right to win" in the industry [22]. The future possibilities for using big, connected data in reliability applications are unbounded. Lifetime models that are based on this data have the potential to explain much more variability in field data than has been possible before. As of today, rarely any solutions on component or system level are available except from high-end products (e.g. in avionics and energy infrastructure). Search for early warning failure indicators is still at a basic research stage. In this chapter, we focus on a PHM that is developed based on the physics of failure of an outdoor driver system used in a lighting application. The typical driver is shown in Fig. 13.1, which consists of a few hundreds of electronics devices, such as transistors, capacitors, resistors, and so on. In a typical outdoor lighting system, in addition

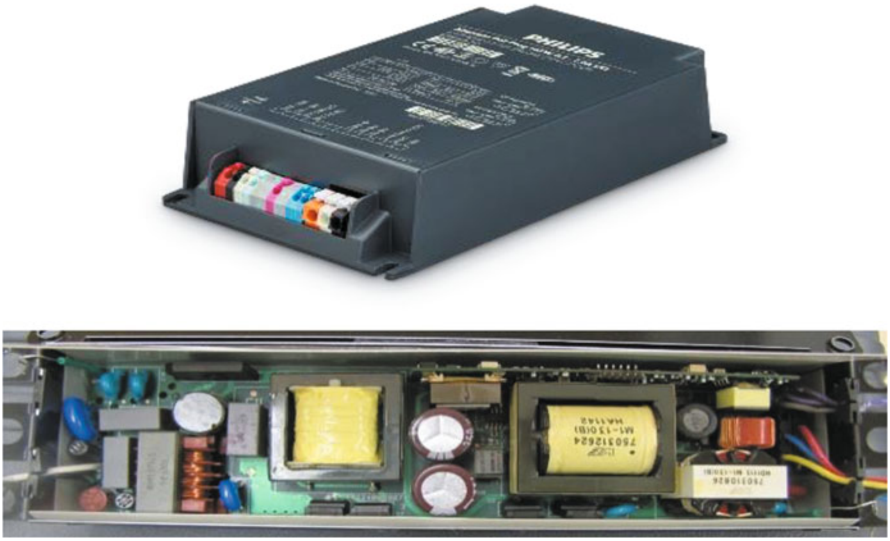

Fig. 13.1 Typical outdoor drivers used in street lighting system

to light module with luminaires, the driver is a key subsystem. It is a critical part of the whole lighting system to reach the targeting lifetime (reliability) in the outdoor applications. Potting compounds are applied in such drivers to help cooling it under very hot days and protect its components from moisture ingress. However, the weakest link of the outdoor driver system is the failure of interconnect due to mechanical stress of potting compounds under extreme conditions. The objective of our work is to monitor the status of degradation of the driver system and then predict the remaining lifetime of the driver. To obtain this objective, we performed tensile and creep tests of a commercially available solder alloy to fit to the Garofalo-Arrhenius creep model [23]. The dynamic mechanical analysis (DMA) tests are performed to derive the storage modulus (E') and glass transition temperature (T_g) of the potting compounds. Then, FEM thermo-mechanical simulations are performed to study the effect of solder and potting compounds on the thermal fatigue properties of solder interconnects [24]. Finally, a first step into PHM of solder interconnect fatigue in potted drivers is presented in this chapter.

13.2 Solder Characterization

An Instron 5948 micro-mechanical tester was utilized to perform tensile tests and creep tests of solder materials at three temperatures (25 °C, 75 °C, 125 °C). Figure 13.2 shows the system and the schematic diagram of the test samples for tensile and creep tests. The dimension of the samples is 3 mm × 0.5 mm × 100 mm. The gauge length is set up to 25 mm. An Instron chamber with Eurotherm 2408 controller is used to heat the sample to the target temperature. A thermometer is installed inside the chamber to measure the temperature during the tests. In addition, cooled water is pumped within the system via chiller to avoid overheating of load cell and actuator.

Firstly, uniaxial tensile tests were performed with a strain rate of 0.001 s^{-1} to determine the stress-strain curves of the solder alloys under different temperatures (25 °C, 75 °C, 125 °C). Three specimens were tested for each temperature level. Then, four creep stress levels were determined based on ultimate tensile strength (UTS) measured from tensile tests, which were 0.25UTS, 0.35UTS, 0.45UTS, and 0.55UTS, respectively. After that, creep tests were performed under three temperatures (25 °C, 75 °C, 125 °C).

13.2.1 DMA Tests of Potting Compounds

Potting compound is a viscoelastic material, for which the stress-strain curve is strongly influenced by temperature. The elasticity of potting compounds will decrease with the increase of temperature, while the viscidity will increase, which means the strain response will be delayed with the increase of temperature.

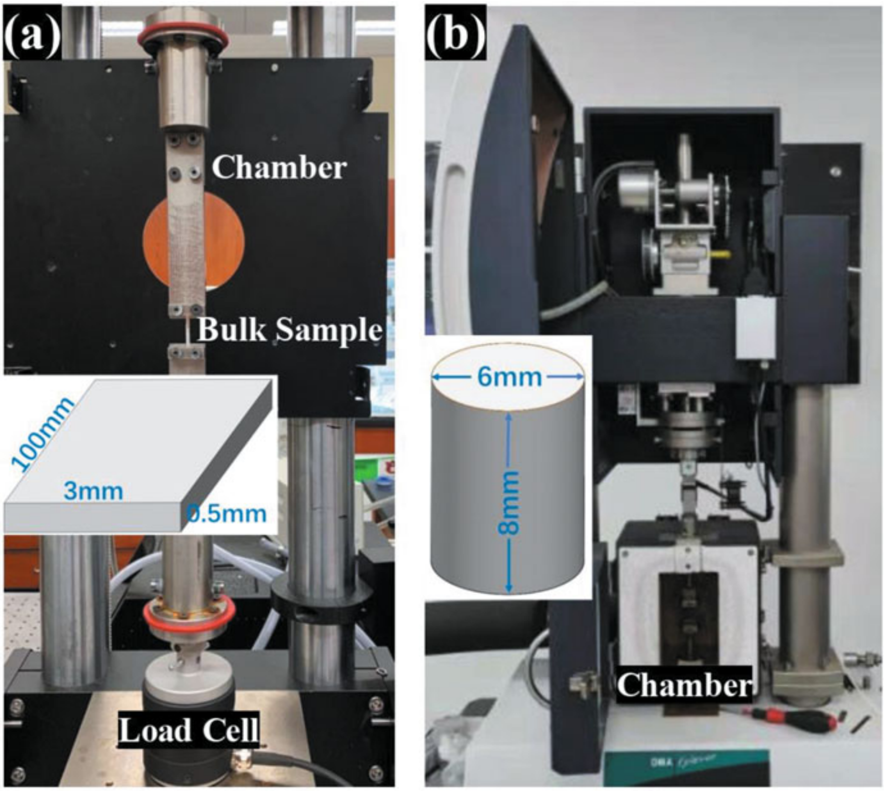

Fig. 13.2 (**a**) Instron 5948 test machine with diagram of tensile and creep specimens; (**b**) dynamic mechanical analysis test machine with the diagram of specimens

Generally, viscoelasticity can be investigated by DMA tests, in which the sample is subjected to oscillating force and the resultant displacement is measured. The storage modulus, *E'*, refers to the stored energy in the material and represents the elastic portion. Loss modulus, *E"*, is a measure of the energy which is dissipated as heat during displacement and represents the viscous portion [25]. It is obvious that the higher the loss modulus, the greater the viscous portion and the higher energy dissipation of the material. To study the effect of potting compounds on thermal fatigue properties of solder interconnects, it is necessary to get the storage modulus and loss modulus of potting compounds. DMA tests are performed for three types of potting compounds (Potting A, Potting B, Potting C) over a temperature range of −50 °C to 30 °C. The test frequency is set as 3 Hz.

13.2.2 *Effect of Temperature on Tensile and Creep Properties of Solder Materials*

The stress-strain curves under three temperatures (25 °C, 75 °C, 125 °C) are shown in Fig. 13.3. Here, the values of UTS show significant decrease with the increase of temperature. When the temperature increases from 25 °C to 75 °C, the UTS decreases from 47.2 MPa to 37.2 MPa. And the UTS continues to decrease down to 25.5 MPa when temperature increases up to 125 °C. This agrees with the following: higher temperature will deteriorate the strength of solder materials. The elongation locates in the range of 2.5% to 8%. It seems that the elongation is not sensitive to temperature change from 25 °C to 75 °C if we ignore the discreteness. But the higher temperature of 125 °C will influence the homogeneity of elongation significantly. Figure 13.3d shows a comparison between SnBiAgCu and SAC305 solder alloys. It is obvious that the strengths of SnBiAgCu are higher than SAC305 solder alloys but the elongation is lower than those of SAC305 solder alloys. It can be concluded

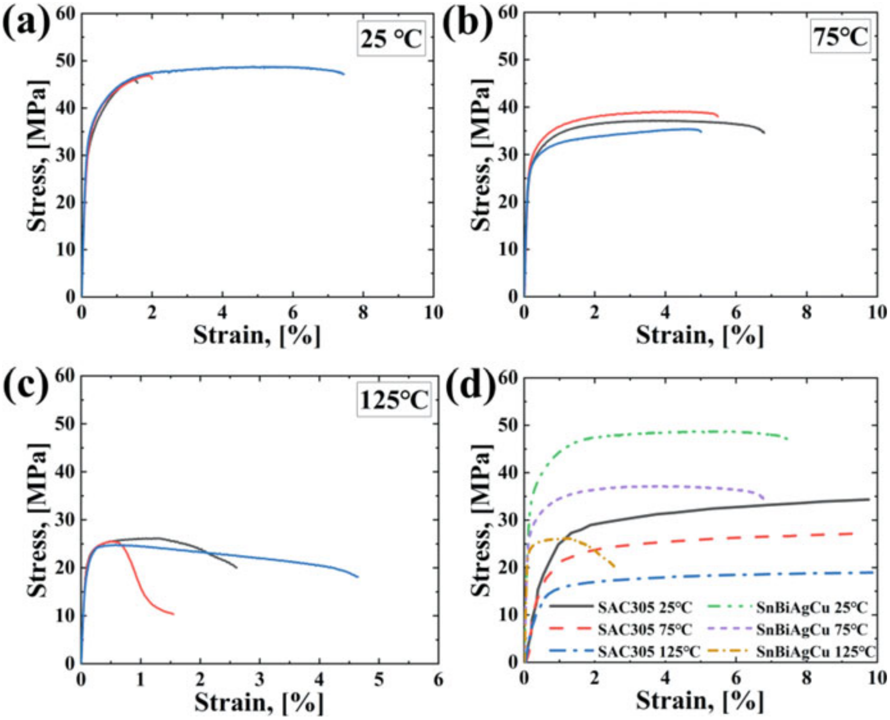

Fig. 13.3 Uniaxial tensile curves of solder materials under different temperatures: (**a**) SnBiAgCu, 25 °C; (**b**) SnBiAgCu, 75 °C; (**c**) SnBiAgCu, 125 °C; and (**d**) comparison between SnBiAgCu and SAC305 solder alloys

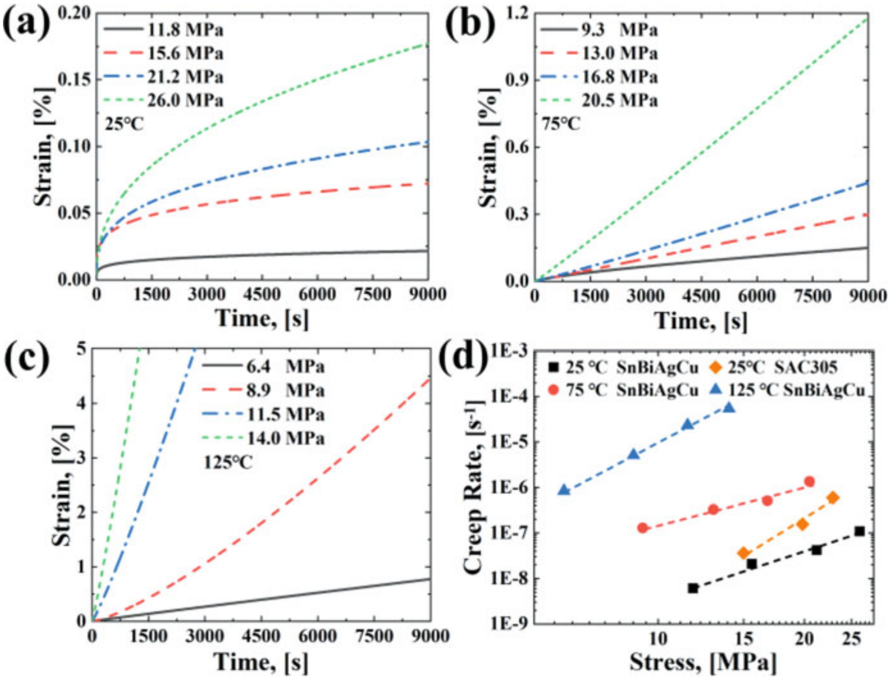

Fig. 13.4 Creep curves of solder alloys under different temperatures: (**a**) SnBiAgCu, 25 °C; (**b**) SnBiAgCu, 75 °C; (**c**) SnBiAgCu, 125 °C; and (**d**) creep rate of SnBiAgCu and SAC305

that the adoption of Bi atom increases the strength of solder but deteriorates the plasticity.

The creep-time curves of solder specimens (SnBiAgCu) under different temperature are provided in Fig. 13.4a–c. It is shown from Fig. 13.4a that sigmoidal creep would occur at low temperature (25 °C) where there would be less thermal activation energy with which to increase an initially low defect density. While at higher temperatures, thermal activation would assist defect generation and/or motion, thereby eliminating the incubation period that characterizes the sigmoidal shape [26, 27]. Therefore, the strain-time curves shown in Fig. 13.4b, c suggest that the typical sigmoidal shape of creep curves disappears. Figure 13.4d shows the steady creep rate of solder specimens under different temperatures which is calculated from creep curves. The values of creep rate were used to fit the constants of the Garofalo-Arrhenius creep model and the results are shown in Table 13.1. Here, we also list the constants of SAC305 according to Schubert et al. [9]. The effect of SnBiAgCu solder alloys compared with SAC305 solder alloys in terms of averaged inelastic strain energy density increment will be calculated in the following section. Figure 13.4d also shows the steady creep rate of SAC305 solder alloys at the temperature of 25 °C, which is higher than that of SnBiAgCu solder alloys obviously. Combining the results from tensile tests and creep tests, it can be

Table 13.1 Constants for Garofalo-Arrhenius creep model

Constants	SAC305	SnBiAgCu
A	277984 s^{-1}	4.03E10 s^{-1}
α	0.02447 MPa^{-1}	0.08771 MPa^{-1}
n	6.41	3.159
Q	5.4E4 J/mol	1.18E5 J/mol

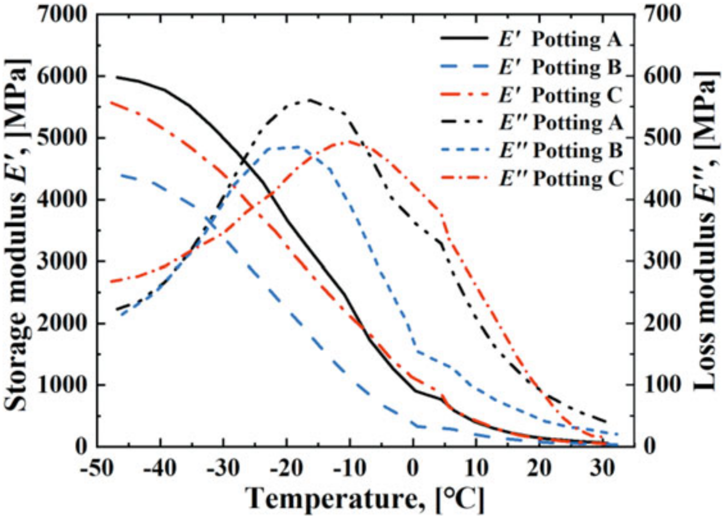

Fig. 13.5 Temperature dependence of the DMA curves of storage modulus *E*' and loss modulus *E*" for the potting compounds

concluded that SnBiAgCu solder alloys present higher strength and creep endurance than SAC305 solder alloys.

13.2.3 DMA Curves of Potting Compounds

Figure 13.5 presents DMA curves of the three potting compounds, which are named as Potting A, Potting B, and Potting C, respectively. The storage modulus (*E'*) denotes the stiffness of the material, which represents the capacity of a material to bear a load. The loss modulus (*E"*) refers to the energy dissipation or the heat loss at the same strain amplitude of a different system. It is shown that as the temperature is raised, the values of *E'* for all types of the potting compounds are diminished. The temperature-storage modulus relationship was due to the increase in the molecular mobility, which lowered the rigidity of the potting compounds and eased their deformation. The stiffness of potting compounds is in order of Potting A, Potting C, and Potting B, which means that Potting A presents higher stiffness than others. It is widely known that the peaks of the loss modulus curves indicate the glass transition temperature (T_g) value of the potting compounds. Thus, the Potting B presents the lowest value of T_g which is about −20 °C, while the T_g values of Potting A and Potting C are −17 °C and −10 °C, respectively. Generally, potting compounds show high CTE at temperatures above their T_g. When low CTE potting compounds are heated past their T_g, the large expansion could subject solder interconnects to excessive bending and normal stresses and lead to accelerated failure of components [28]. It is thus important to optimize the CTE of potting compounds close to the solder materials and to adjust the T_g according to their real application environment.

13.3 Finite Element Simulations

A FEM simulation is used to compute the thermal-mechanical stresses and strain response of the solder interconnects while undergoing thermal cycling. The study focuses on a commercially available package with gull-wing leads (SOD323) and a diode frequently utilized in LED drivers. As illustrated in Fig. 13.6, Ansys Workbench is employed to develop a three-dimensional (3D) finite element model representing one-quarter of the package. A substructure technique is employed to enhance the FEM calculation efficiency without sacrificing accuracy. Notably, the displacement is set as 0 in directions perpendicular to the symmetric planes, and the

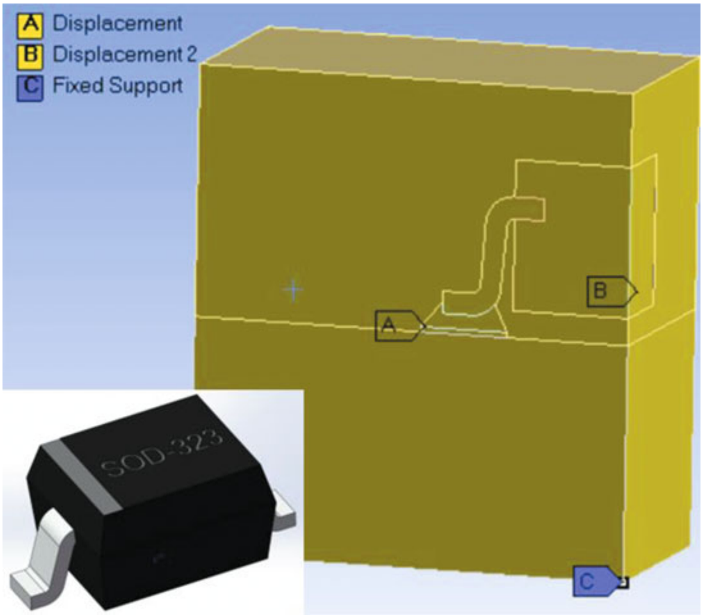

Fig. 13.6 Schematic of a quarter of SOD323 model used in FEM and boundary condition

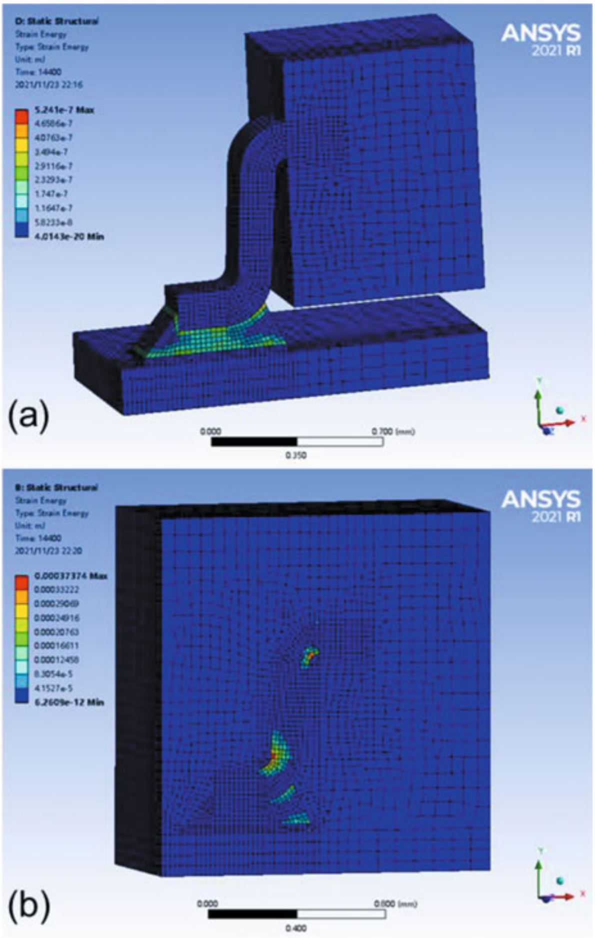
D: Static Structural
Strain Energy
Type: Strain Energy
Unit: mJ
Time: 14400
2021/11/23 22:16
5.241e-7 Max
4.6586e-7
4.0763e-7
3.494e-7
2.9116e-7
2.3293e-7
1.747e-7
1.1647e-7
5.8233e-8
4.0143e-20 Min
ANSYS
2021 R1
(a)
0.000
0.700 (mm)
0.350
B: Static Structural
Strain Energy
Type: Strain Energy
Unit: mJ
Time: 14400
2021/11/23 22:20
0.00037374 Max
0.00033222
0.00029069
0.00024916
0.00020763
0.00016611
0.00012458
8.3054e-5
4.1527e-5
6.2609e-12 Min
ANSYS
2021 R1
(b)
0.000
0.800 (mm)
0.400

Fig. 13.7 Strain energy density distribution (**a**) without potting; (**b**) with potting

vertex located at the intersection of the symmetric planes, as shown in Fig. 13.6, is kept fixed.

As the solder interconnects are expected to undergo creep deformation under thermal cyclic conditions, the Garofalo-Arrhenius creep model [9] is employed to simulate their creep behaviour. The temperature range is −40 to 120 °C. And the initial temperature is set as 120 °C. As the inelastic strain energy density per cycle is stable after three cycles, four cycles were performed in the FEM simulations. The strain energy distribution at the end of fourth cycle within the solder interconnect is illustrated in Fig. 13.7. Figure 13.7a shows the strain energy of the component without potting materials. Figure 13.7b shows the strain energy of the component with potting materials. It indicates that the highest amount of energy is concentrated in the solder interconnect without potting materials. The mechanical properties of solder present high temperature sensitivity. The creep deformation accounts for the

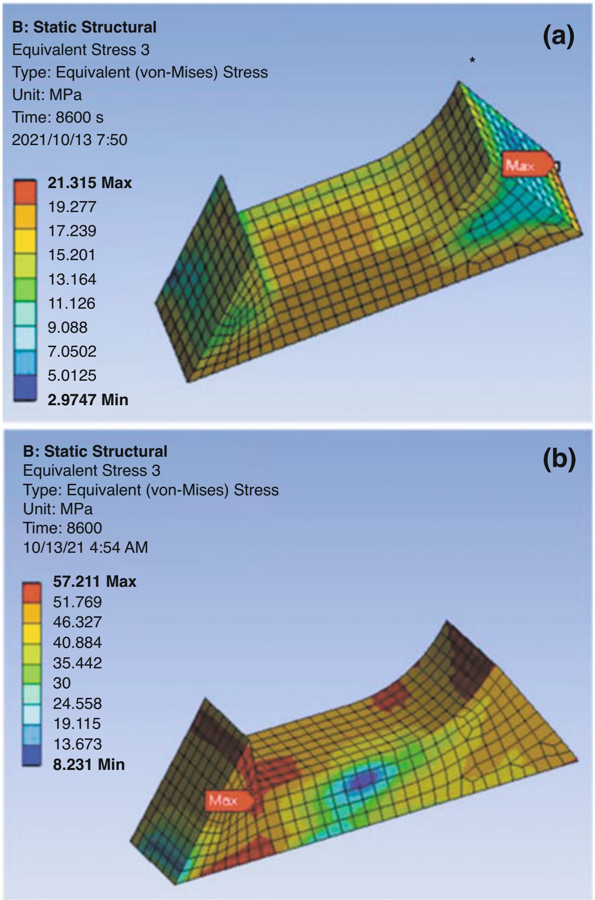
B: Static Structural
Equivalent Stress 3
Type: Equivalent (von-Mises) Stress
Unit: MPa
Time: 8600 s
2021/10/13 7:50
(a)
21.315 Max
19.277
17.239
15.201
13.164
11.126
9.088
7.0502
5.0125
2.9747 Min
Max
B: Static Structural
Equivalent Stress 3
Type: Equivalent (von-Mises) Stress
Unit: MPa
Time: 8600
10/13/21 4:54 AM
(b)
57.211 Max
51.769
46.327
40.884
35.442
30
24.558
19.115
13.673
8.231 Min
Max

Fig. 13.8 Stress density distribution (**a**) without potting; (**b**) with potting

main failure mechanism under thermal cyclic condition. While when the solder joints are surrounded by the potting material, the strain energy distribution presents significant difference. The higher strain energy density concentrates at the interface of potting materials and solder joints. This is caused by the CTE mismatch among potting material, solder joint, and Cu lead frame. Figure 13.8 shows the stress distribution of solder joint. Potting materials will cause higher stress inside the solder joints. The shrink under the low temperature and the expansion under the high temperature of the potting materials will induce tensile or compression stress on the solder joints, which produces more plastic deformation. Moreover, the potting material will be very hard when the temperature is lower than its T_g. As the T_g of potting material used in this study is -10 °C, which is higher than the minimum temperature during the thermal cyclic process, low temperature is anticipated to be more harmful than high temperature. To decrease the CTE mismatch, a potting material with lower T_g is very important for the low-temperature application of electronic components.

13.4 Prognostics and Health Monitoring

The PHM method developed intends to monitor and collect data online and work out a model for predicting the life cycles at any user condition. The method is implemented in a LED driver module which allows for collecting failure data under simulated extreme weather conditions. In the cold winter, the lowest temperature in some high-latitude regions can reach −40 °C for few days. In the hot summer, the hot spot in the driver can be up to 80 °C. Figure 13.9 depicts the test equipment used and the driver module used. Simplified drivers are designed and fabricated and then put in an oven with applied high and low temperature which correlates with the extreme environmental conditions in outdoor applications. The drivers are powered cyclically. The exact user conditions, e.g. the temperature around the critical components, are monitored and the status of the degradation is monitored and recorded automatically.

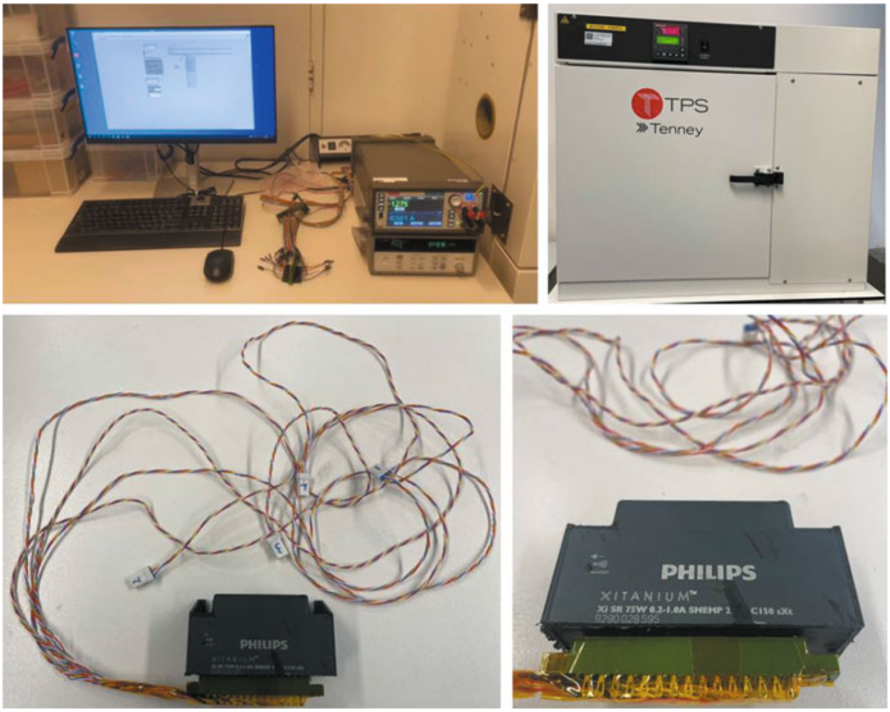

Fig. 13.9 Test equipment (top) and driver modules (bottom) used for PHM

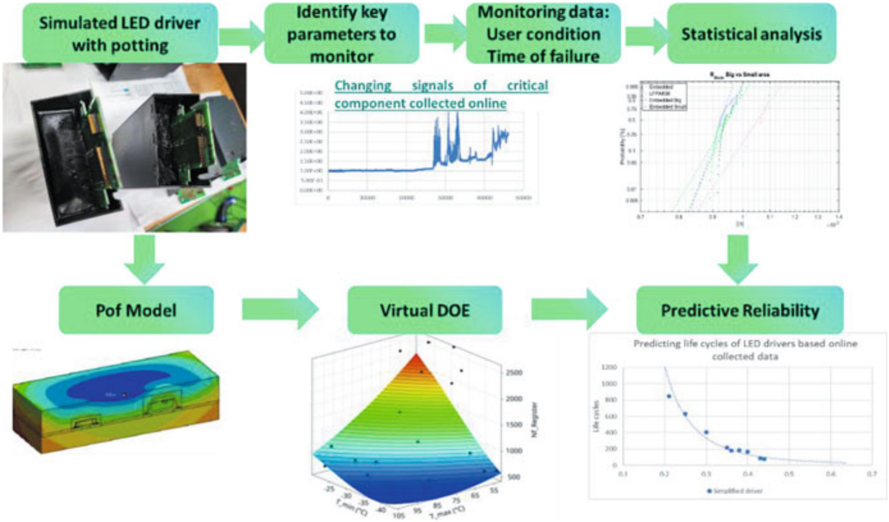
Simulated LED driver with potting
Identify key parameters to monitor
Monitoring data: User condition Time of failure
Statistical analysis
Changing signals of critical component collected online
Pof Model
Virtual DOE
Predictive Reliability
Predicting life cycles of LED drivers based online collected data
Life cycles
Simplified driver
NF_Register
T_min (°C)
T_max (°C)

Fig. 13.10 Flowchart for the PHM-based lifetime prediction

The collected data, especially the data point above certain threshold value, is reported. Based on the above-described FEM simulations for the physics of failure, the critical damage level could be given. The damage level and the collected life data correlate together to form a model for predicting the lifetime of the drivers at certain user condition. Figure 13.10 depicts the flowchart of the PHM-based lifetime predictions for the electronic drivers.

Since the real lifetime of this type of drivers from the field is not available yet, we validated the model by testing a few real drivers in the lab. As being shown in Fig. 13.11, life cycles of the real driver (orange colour) under extreme conditions match well with the predicted cycles out of the model. As a reference, old test data without the online measurement was shown in the figure as well. The predicted life cycles are a bit lower than the current PHM-based method.

13.5 Conclusions

In this chapter we describe the combination of experimental material characterization with numerical FEM simulations to obtain a PHM methodology for interconnect failures in LED drivers. Solder fatigue is a key failure mode in the electronic industry. Monitoring the actual degradation of the solder under real-time conditions in any application would be extremely beneficial. As input for the FE models, experimental characterization of a new type of solder is described. To enable the PHM, a FE model is created of a typical component in electronic drivers. The calculated damage level and the collected life data correlate together and form

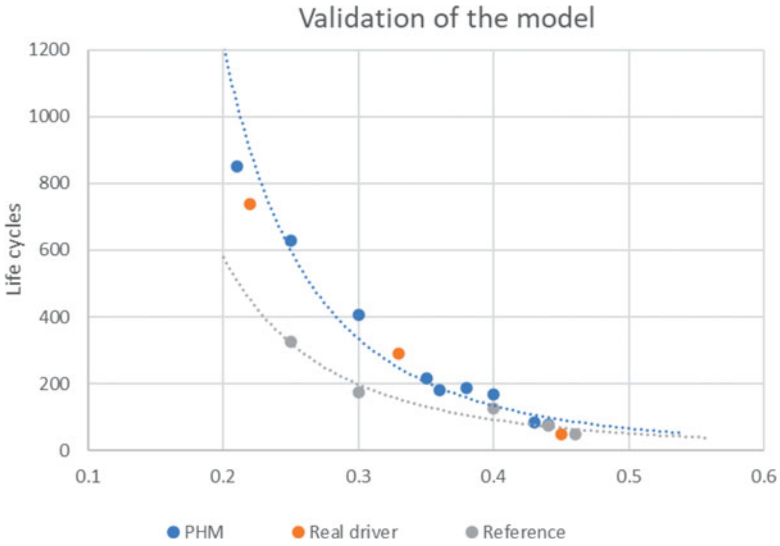

Fig. 13.11 Validation of the PHM-based lifetime model

a model for predicting the lifetime of the drivers at certain user condition. The developed PHM methodology helps in identifying and reporting the failure of the driver in real time. The developed model is very useful for predicting the actual remaining useful life (RUL) of current outdoor LED drivers. The intention is to install such a system in real connected lighting systems which can store the detected data in the cloud.

Acknowledgments This project has received funding from the ECSEL Joint Undertaking (JU) under grant agreement No 876659. The JU receives support from the European Union's Horizon 2020 research and innovation programme and Germany, Austria, Slovakia, Sweden, Finland, Belgium, Italy, Spain, Netherlands, Slovenia, Greece, France, and Turkey.

References

1. Fang, L., Bo, J., & Wei, T. (2016). *Review of board-level solder joint reliability under environmental stress*. Prognostics and System Health Management Conference (PHM-Chengdu), Chengdu, China (pp. 1–6). https://doi.org/10.1109/PHM.2016.7819918.
2. Coyle, R. J., Sweatman, K., & Arfaei, B. (2017). Thermal fatigue evaluation of Pb-free solder joints: Results, lessons learned, and future trends. *JOM, 67*, 2394–2415.
3. Cai, Z., Zhang, Y., Suhling, J. C., Lall, P., Johnson, R. W., & Bozack, M. J. (2010). *Reduction of lead-free solder aging effects using doped SAC alloys*. ECTC (pp. 1493–1511).
4. Yang, L., Zhu, L., Zhang, Y., Zhou, S., et al. (2019). Microstructure, IMCs layer and reliability of Sn-58Bi solder joint reinforced by Mo nanoparticles during thermal cycling. *Materials Characterization, 148*, 280–291.

5. Guo, F., Choi, S., Subramanian, K. N., Bieler, T. R., Lucas, J. P., Achari, A., & Paruchuri, M. (2003). Evaluation of creep behaviour of near-eutectic Sn-Ag solders containing small amount of alloy additions. *Materials Science and Engineering A, 351*, 190–199.
6. Shen, L., Tan, Z. Y., & Chen, Z. (2013). Nanoindentation study on the creep resistance of SnBi solder alloy with reactive nano-metallic fillers. *Materials Science and Engineering A, 561*, 232–238.
7. Lee, W., Nguyen, L. T., & Selvaduray, G. S. (2000). Solder joint fatigue models: Review and applicability to chip scale packages. *Microelectronics Reliability, 40*(2), 231–244.
8. Wong, E. H., van Driel, W. D., Dasgupta, A., & Pecht, M. (2016). Creep fatigue models of solder joints: A critical review. *Microelectronics Reliability, 59*, 1–12., issn: 0026-2714. https://doi.org/10.1016/j.microrel.2016.01.013
9. Schubert, A., Dudek, R., Auerswald, E., Gollhardt, A., Michel, B., & Reichl, H. (2003). *Fatigue life models for SnAgCu and SnPb solder joints evaluated by experiments and simulation.* ECTC.
10. Athamneh, R. A., Hani, D. B., Ali, H., & Hamasha, S. (2020). Fatigue life degradation modelling of SnAgCu solder joints after aging. *IEEE Trans Compon Packaging Manuf Technol, 10*, 1175–1184.
11. Alam, M. S., Suhling, J. C., & Lall, P. (2016). *High temperature tensile and creep behaviour of lead-free solders*. IEEE ITHERM (pp. 1218–1224).
12. Samavatian, V., Eini, H. I., Avenas, Y., & Samavatian, M. (2020). Effects of creep failure mechanisms on thermomechanical reliability of solder joints in power semiconductors. *IEEE Transactions on Power Electronics, 35*, 8956–8964.
13. Long, X., Tang, W., Xu, M., Keer, L. M., & Yao, Y. (2018). Electric current assisted creep behaviour of Sn–3.0Ag–0.5Cu solder. *Journal of Materials Science, 53*, 6219–6229.
14. Dokoupil, J., & Stary, J. (2021). Effect of temperature cycling on IMC growth and solder joint strength of SAC305 solder alloy and low silver alloy REL61. *ECS Transactions, 105*, 391–400.
15. Serebreni, M., Wilcoxon, R., & McCluskey, F. P. (2018). *Modelling the influence of conformal coatings on thermo-mechanical fatigue of solder interconnects in electronic packages*. HiTEC (pp. 000007–000014).
16. Serebreni, M., Blattau, N., Sharon, G., & Hillman, G. (2017). *Effect of encapsulation materials on tensile stress during thermo mechanical cycling of Pb-free solder joints*. IPC APEX.
17. Zhu, J., Bellini, M. O., Chicharro, D. M., Betts, T. R., & Gottschalg, R. (2018). Effect of viscoelasticity of ethylene vinyl acetate encapsulants on photovoltaic module solder joint degradation due to thermomechanical fatigue. *Japanese Journal of Applied Physics, 57*.
18. Lall, P., Lowe, R., & Goebel, K. (2012). Prognostics health management of electronic systems under mechanical shock and vibration using Kalman filter models and metrics. *IEEE Transactions on Industrial Electronics, 59*(11), 4301–4314.
19. Kwon, D., Azarian, M. H., & Pecht, M. (2015). Remaining-life prediction of solder joints using RF impedance analysis and Gaussian process regression. *IEEE Transactions on Components Packaging and Manufacturing Technology, 5*(11), 1602–1609.
20. Pecht, M. G. (2008). *Prognostics and health management of electronics*. John Wiley & Sons.
21. Meeker, W. Q., & Hong, Y. (2013). Reliability meets big data: Opportunities and challenges. Statistics Preprints. Paper 82. http://lib.dr.iastate.edu/stat_las_preprints/82.
22. Van Driel, W. D., Fan, X. J., & Zhang, G. Q. Solid state lighting reliability – part II, 07/2017; Springer, 978-3-319-58174-3, https://doi.org/10.1007/978-3-319-58175-0.
23. Du, L., Zhao, X., Poelma, R., Van Driel, W., & Zhang, G. (2023). *High-temperature creep properties of a novel solder material and its thermal fatigue properties under potting material*. 2023 IEEE 73rd Electronic Components and Technology Conference (ECTC), Orlando, FL, USA (pp. 392–395). https://doi.org/10.1109/ECTC51909.2023.00072.
24. Du, L., Zhao, X., Watté, P., Poelma, R., Van Driel W., & Zhang G. (2022). *Investigation of potting compounds on thermal-fatigue properties of solder interconnects*. IECON 2022 – 48th Annual Conference of the IEEE Industrial Electronics Society, Brussels, Belgium (pp. 1–5). https://doi.org/10.1109/IECON49645.2022.9968578.

25. Ernst, L. J., Zhang, G. Q., Jansen, K. M. B., & Bressers, H. J. L. (2003). Time- and temperature-dependent thermo-mechanical modelling of a packaging moulding compound and its effect on packaging process stresses. *ASME Journal of Electronic Packaging, 125*(4), 539–548. https://doi.org/10.1115/1.1604156
26. Fan, X., Pei, M., & Bhatti, P. K. (2006). *Effect of finite element modelling techniques on solder joint fatigue life prediction of flip-chip BGA packages*. ECTC.
27. Shangguan, D. (2005). *Lead-free solder interconnect reliability*. ASM International.
28. Lee J., Hwang T. K., Kim J. Y., et al. 2007. *Study on the board level reliability test of package on package (PoP) with 2nd level underfill*. ECTC.